PNE-906
FINAL REPORT

Plowshare civil, industrial and scientific uses for nuclear explosives

UNITED STATES ATOMIC ENERGY COMMISSION / PLOWSHARE PROGRAM

NEVADA TEST SITE

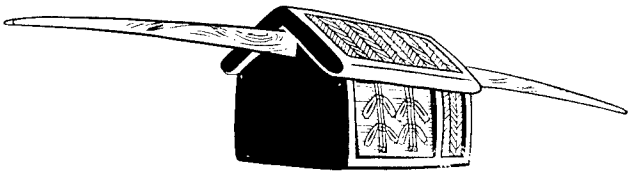

Palanquin

NEVADA
CALIFORNIA
MERCURY
LAS VEGAS

Preshot Geophysical Properties of Palanquin Crater Site

University of California
Lawrence Radiation Laboratory

Mercury, Nevada & Livermore, California ISSUED: OCTOBER 11, 1968

LEGAL NOTICE

Printed in USA. Price $3.00. Available from the Clearinghouse for Federal Scientific and Technical Information, National Bureau of Standards, U. S. Department of Commerce, Springfield, Virginia 22151.

USAEC Division of Technical Information Extension, Oak Ridge, Tennessee

PNE-906
NUCLEAR EXPLOSIONS-PEACEFUL
APPLICATIONS (TID-4500)

PROJECT PALANQUIN

PRESHOT GEOPHYSICAL PROPERTIES OF PALANQUIN CRATER SITE

Ronald T. Stearns
G. Lewis Meyer

Lawrence Radiation Laboratory
Mercury, Nevada

Spenst M. Hansen

Lawrence Radiation Laboratory
Livermore, California

January 1968

This report has also been issued as UCRL-50411.

Contents

Acknowledgments

The authors are grateful to the following organizations and individuals assisting in the collection and evaluation of data included in this report:

Borehole Photography

Go-Western Logging and Perforating Company, Bakersfield, California

Drilling Records

C. Drake and W. Hackler of the Waterways Experiment Station U. S. Army Corps of Engineers, Vicksburg, Mississippi

Geological Mapping and Lithogical Descriptions

Donald C. Noble and Bruce V. Hanson, U. S. Geological Survey, Special Porjects Branch, Denver, Colorado

Richard Hunt, Geologist, Waterways Experiment Station, U. S. Army Corps of Engineers, Vicksburg, Mississippi

Geophysical Logging

Welex Division, Hailliburton, Inc. , Tulsa, Oaklahoma

Seismic Logging

R. C. Carlson and J. T. Cherry, Lawrence Radiation Laboratory.

PRESHOT GEOPHYSICAL PROPERTIES OF PALANQUIN CRATER SITE

Abstract

The Palanquin nuclear cratering experiment was conducted on April 14, 1965 at the Nevada Test Site of the U. S. Atomic Energy Commission. Eight preshot holes were drilled which consisted of the emplacement hole, two instrument holes, and five exploratory holes. The maximum depth reached was 187 m.

The rocks at the Palanquin site are of volcanic origin, and consist predominantly of trachyte porphyry of the Ribbon Cliff formation of Pliocene age. Pyroclastic volcanic tuff underlies the trachyte porphyry at a depth of 175 m and caps low hills adjacent to the site. The volcanic units have a general horizontal attitude, although flow structures show gentle-to-steep dips. No ground water was encountered.

The physical properties of the trachyte porphyry medium show considerable variation. Zones of jointing and brecciation are widespread, particularly in the upper 60 m, with caliche and clay surrounding blocks and fragments of rock. These zones caused severe out-of-gauge conditions in the drill holes, and poor recovery. No evidence of faulting in the vicinity of surface ground zero was found.

Logs used in the drill holes of the Palanquin site were the gamma-gamma density, caliper, seismic velocity, drilling and coring time, and percent core recovery. These logs were made with instruments furnished by and operated by the Welex Division. Logs were also constructed from drilling and coring penetration rates, and from percent core recovery. In situ sonic velocity measurements were made in several of the drill holes. All logs were run in open, dry holes, since the highly fractured rock medium precluded filling the holes with fluid.

In situ velocity measurements were made using the seismic uphole logging technique developed at the Lawrence Radiation Laboratory. Average velocities of 907 and 2,427 m/sec were measured. A velocity discontinuity was located at a depth of approximately 27 m.

Measurements of in situ physical properties at nuclear experiment sites prior to the investigations at Palanquin were sparse. The geophysical measurements at the Palanquin site assisted in the development of improved techniques, and demonstrated the need for high-resolution logging tools and methods.

Introduction

The Palanquin nuclear-explosion cratering experiment was conducted at Area 20 of the AEC Nevada Test Site, Nye County, Nevada. This experiment was part of the program sponsored by the AEC, and carried out by the Lawrence Radiation Laboratory (LRL) for the investigation of nuclear cratering technology. The device fired on April 14, 1965, at 0514 (PST), consisted of a 4.3 ± 0.3 kt nuclear explosion. The emplacement hole was situated at geodetic coordinates: longitude W116°31'24.80", latitude N37°16'49.35". A nuclear crater resulted with an apparent-crater radius of 36.3 m and an apparent-crater depth of 24.0 m. The volume of the apparent crater was 35,569 m^3.

Geophysical measurements and observations included in this report are:

(1) Welex gamma-gamma density log
(2) Welex caliper log
(3) Seismic hole-to-hole survey
(4) Seismic uphole survey
(5) Seismic refraction survey
(6) Drilling time log
(7) Percent core recovery log
(8) Downhole stereophotography

A description of the geologic environment has also been included.

Site Description

The Palanquin site is situated in the northwest corner of Area 20, Pahute Mesa, of the AEC Nevada Test Site, Nye County, Nevada (see Fig. 1). The Nevada State coordinates are N921,072, and E541,636. The surface elevation of ground zero was 1,888 m above sea level.

The surface ground zero (SGZ) was near the end of a gently sloping, southward-trending ridge. This ridge is approximately 900 m long and 450 m wide. In general, the topography within an approximate radius of 3,000 m of the Palanquin SGZ is gently rolling hills and valleys (see Fig. 2).

Eight holes were drilled at the site during February and March, 1965. Table I tabulates data from these. Hole U20k has the Nevada State coordinates given above for the Palanquin experiment. The location of the balance of the holes and their relationship to one another is shown in Fig. 3.

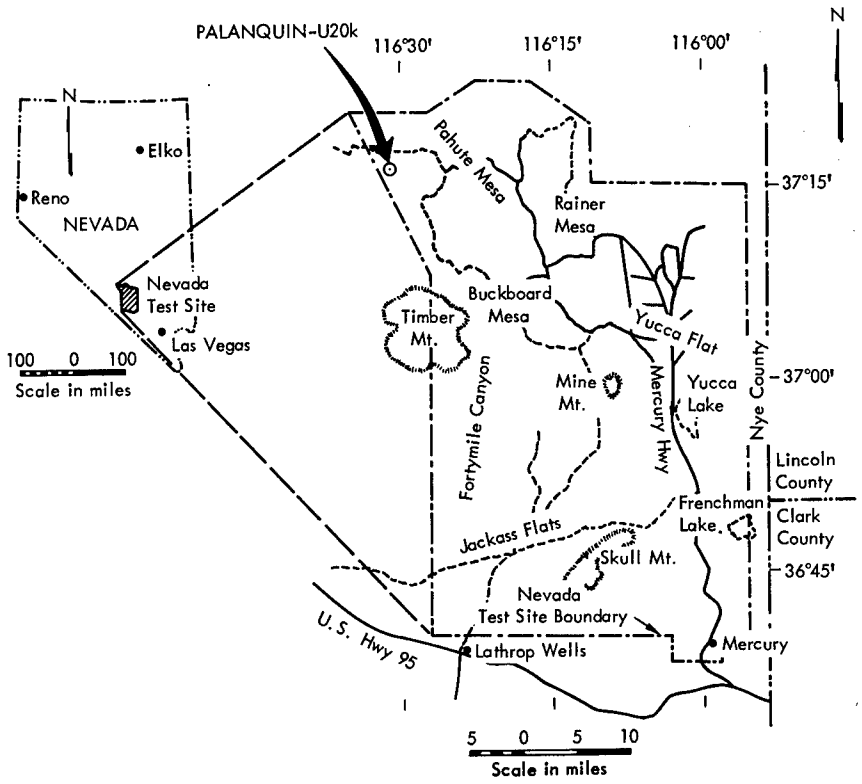

Fig. 1. Location map of Palanquin nuclear crater experiment.

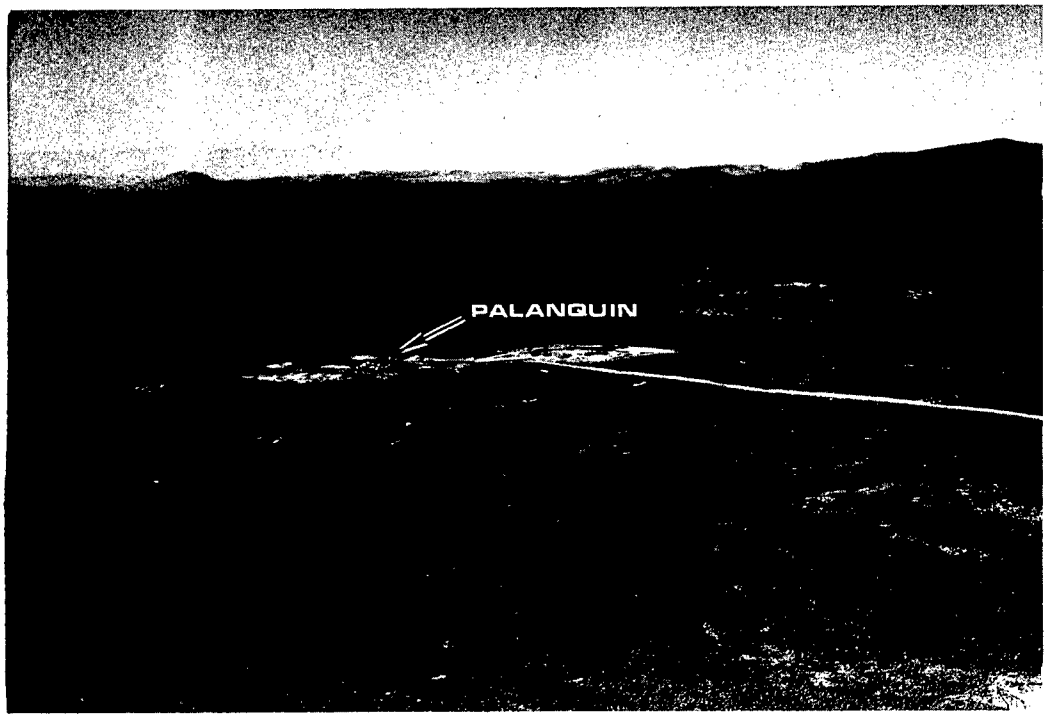

Fig. 2. Aerial photograph of Palanquin site looking southerly. Note low flat hills south of crater site capped with ash flow tuff beds of Thirsty Canyon formation.

Table I. Data on preshot drill holes at Palanquin site.

Hole	Purpose	Size	Surface elevation (m)	Depth (m)	Core	WES borehole photography interval (m)	Laval borehole photography interval (m)	Caliper log interval (m)	Density log interval (m)	Drilling time log interval (m)
U20k	Emplacement	122 cm	1887.9	187.5	None	None	0-101	1-183	None	6-187
U20k-1	Instrument	25 cm	1887.9	107	None	None	0-107	2-106	0-107	12-102
U20k-2	Instrument	25 cm	1879.2	149	None	None	0-122	0-149	0-149	10-149
Ue20k-1	Exploratory	14 cm	1887.9	107.0	Continuous	1-107	None	0-107	0-107	1-104
Ue20k-2	Exploratory	NX[a]	1885.2	82.3	Continuous	1-82	None	None	None	2-82
Ue20k-3	Exploratory	NX	1884.3	82.4	Continuous	2-82	None	None	None	6-83
Ue20k-4	Exploratory	NX	1887.0	60.7	Continuous	11-55	None	None	None	4-61
Ue20k-5	Exploratory	NX	1887.9	66.4	Continuous	None	None	None	None	4-61

[a]NX = 7.5-cm drill size.

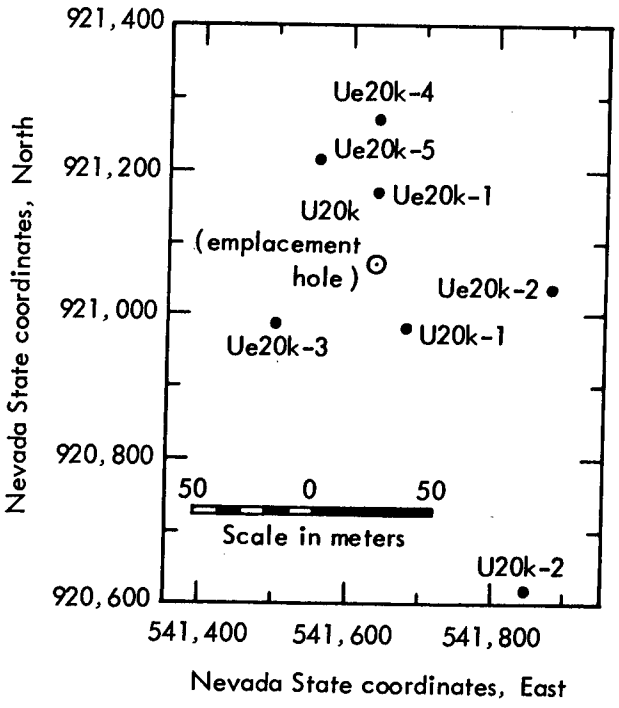

Fig. 3. Location map for drill holes at Palanquin site.

Geology

General

The rocks at the Palanquin site are of volcanic origin. The Ribbon Cliff formation* of Pliocene age is exposed at the surface and is 185 m thick. It is underlain by softer volcanic rock, probably a basal breccia which is transitional to the Timber Mountain tuff formation. The volcanic units have a general horizontal attitude, although flow-bedding within the units locally shows steep-to-gentle dips. Weathered rock and shallow soil with thickness typically from 0.5 to 5 m obscure most of the bedrock surface, making interpretation of jointing and fault structures difficult. There is no definite evidence of faulting within a 300-m radius of the emplacement hole, either from drill core data or from surface mapping. The regional water table is believed to be situated between 400 and 450 m below the land surface. Water was not encountered in any of the drill holes.

Lithology

Three volcanic formations are either exposed at the surface or were penetrated by drilling. These are listed and briefly described below in order of youngest to oldest.

Thirsty Canyon Tuff Formation

This formation is not present at the site itself, but forms thin capping on hills and ridges to the north, west, and south at distances of several hundred meters. None of the outcrops of the Thirsty Canyon are close enough to have a significant effect on the Palanquin experiment.* The lithology consists predominantly of ash flow tuff.

Ribbon Cliff Formation

At the Palanquin site this formation is approximately 185 m thick and consists of a series of lava flows. The predominate rock type is brownish to reddish-brown trachyte porphyry containing approximately 20% light grey phenocrysts of anorthoclase. The rock is highly to moderately vesiculated in the upper zone, the base of which varies in depth from 17 to 66 m. In some instances, a second interval of vesicular lava was encountered below an interval of dense lava. The rock underlying the upper vesiculated zone is predominantly dense trachyte porphyry.

Timber Mountain Tuff Formation

A general description of this unit is included in Orkild and Sargent** and is not repeated here. A softer volcanic rock which appears to be a basal breccia was intersected by drill hole U20k from 185 m to the hole bottom at 199m. This rock was probably transitional to the lower vitric bedded tuffs of the Ammonia Tanks member of the Timber Mountain

*This unit is also referred to in various reports as the Phyolite of Ribbon Cliff or the Lavas of Ribbon Cliff. The designation Ribbon Cliff formation is used in this report.

*The two members of the Thirsty Canyon present in the area are the Trail Ridge member and the Spearhead member. A lithologic description of these units is given by Orkild and Sargent (Ref. 1, p. 3).

**See Ref. 1, pp. 6-7.

formation. Since drill hole U20k was not cored, detailed information on the characteristics of this underlying unit was not obtained. The top of the formation is tentatively placed at 185 m below the surface.

Noble and Hanson inferred the chemical analysis of the trachyte porphyry at the Palanquin site from chemical and spectrographic analyses of samples taken from the Ribbon Cliff formation in nearby areas:*

	Percent
SiO_2	64.0
Al_2O_3	17.0
Fe_2O_3	2.5
FeO	1.7
MgO	0.6
CaO	1.7
Na_2O	5.1
K_2O	5.0
$H_2O \pm 0.8\%$ TiO_2	0.7

Structure

Detailed surface mapping and aerial photogrammetry have identified lineations which are predominantly the result of planar flow structures. These flow structures define an arcuate pattern concave to the west and centered approximately 500 m northwest of U20k. The strike of these features is approximately N55° E, with steep-to-vertical dips. The source of the trachyte porphyry lavas was about 1,500 m easterly from U20k. These flow structures are strongly developed in many outcrops of the Ribbon Cliff. Field examination reveals them to be defined by flow banding, flow parting, flattened gas vesicles, and planar alignment of tabular feldspar phenocrysts.*

A strong east-west trending lineation passing within 40 m south of SGZ was identified from aerial photographs. This feature has a minimum strike length of over 2,000 m and is distinct from the flow structures described above. A possible interpretation is that this lineation is the surface expression of a fault; however, this east-west trend is contrary to known regional structural trends, and its identification as a fault cannot be supported by other evidence.

Primary jointing is widespread in occurrence throughout the Ribbon Cliff. The average fracture density is probably in the range of 3 to 6 fractures/m. Data from the drill core indicate that many of the fractures are partially healed by feldspar, quartz, and amphiboles. Post volcanic cooling deposition of caliche and clay minerals was noted along joints and fractures and in brecciated zones.

The degree of structural inhomogeneity of the rock is very great, particularly near the surface where the lava is vesiculated (see Fig. 4) Considerable alteration of the trachyte to clay along joints has occurred. In the brecciated zones, the Ribbon Cliff can best be described as consisting of blocks and fragments of rock, often vesiculated and porous, packed together in a lattice work of clay. Severe out-of-gauge conditions in several of the drill holes were the result of these blocks caving into the bore. Conditions such as these also are believed to have contributed significantly to the locally poor recovery.

*See Ref. 2, pp. 12-13.

*See Ref. 2, pp. 3-6.

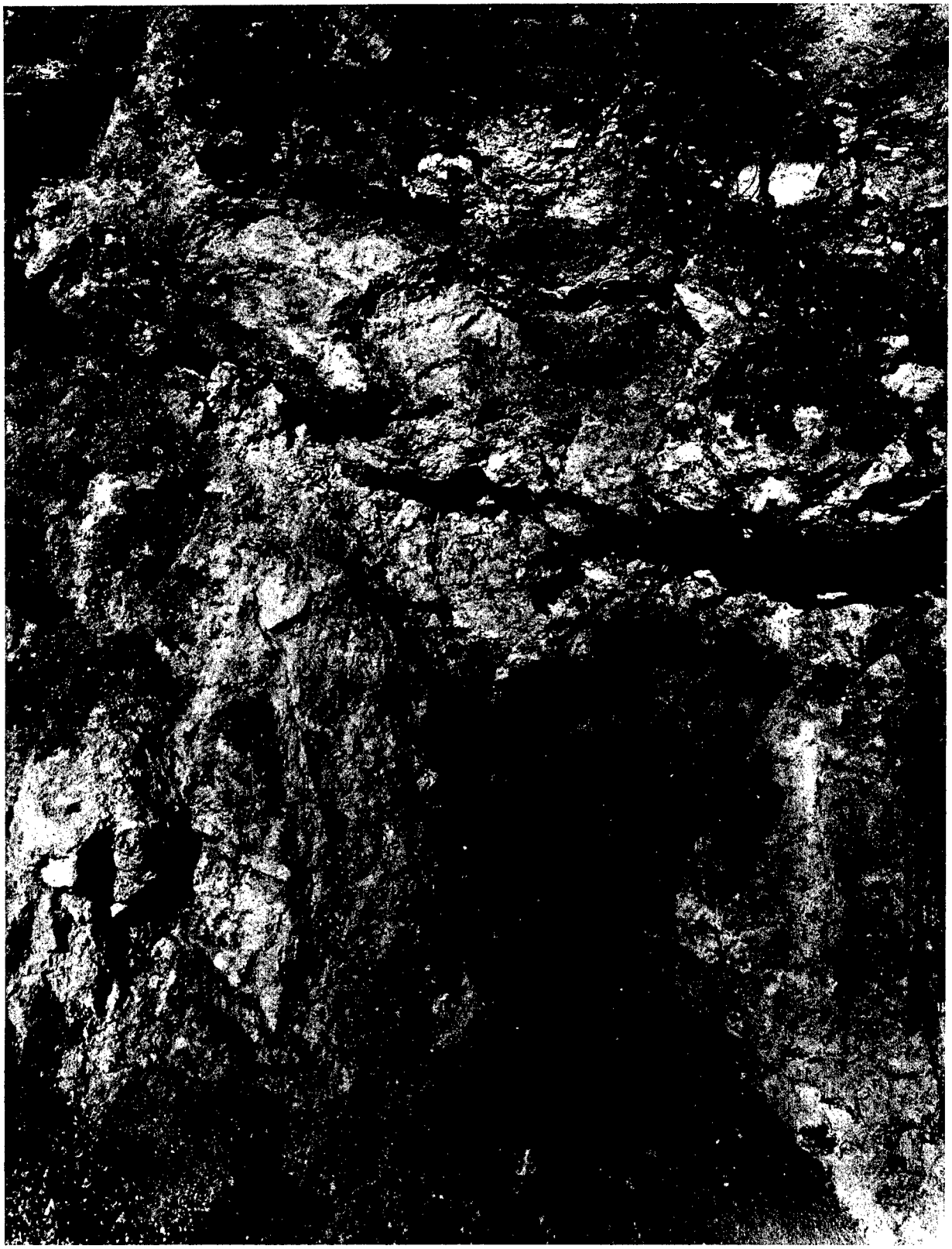

Fig. 4. Rock exposure on side of excavation in vesicular facies of Ribbon Cliff formation at Palanquin site.

Alteration, clay and caliche deposition, and fracturing are controlled only partly by proximity to the surface. Also, incompetent and fractured rock is not continuous in occurrence between the surface and the more dense trachyte porphyry below the vesiculated zone. One of the more highly altered and fractured zones was noted between 43 and 49 m. Several shallow zones consist of 6 to 10 or more m of nearly continuous, competent rock. Vertical fractures are locally numerous and occasionally stand open for widths of 2 cm or more. This is illustrated by the borehole photographs (Fig. 5).

Direct subsurface evidence of faulting is absent. Correlations of such features as gouge, slickensides, or brecciation

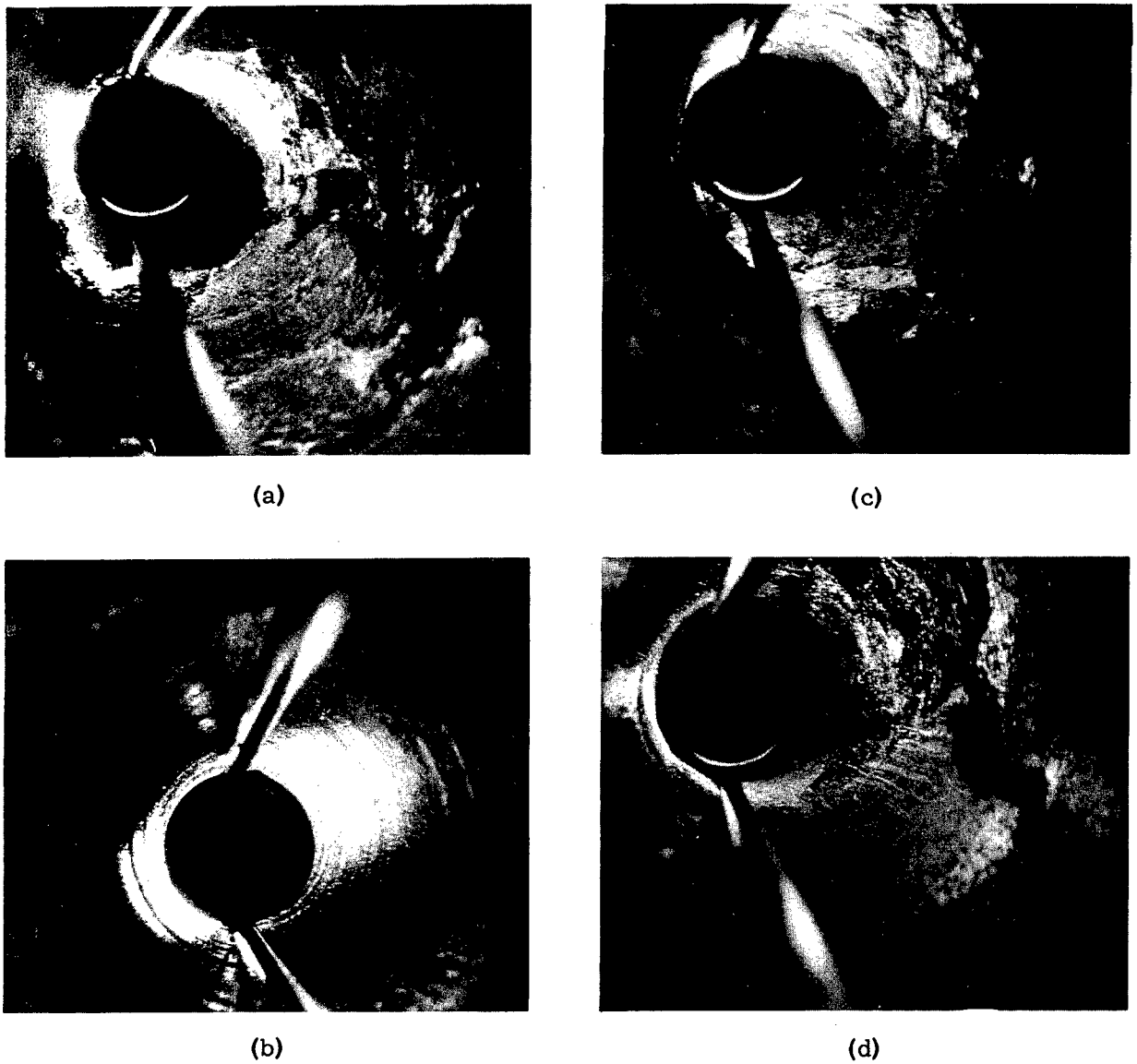

Fig. 5. Borehole photographs taken in Ue20k-1 (borehole diameter, 14 cm). (a) Depth—34.1 m. Note open fracture and hole erosion on right. (b) Depth—36.0 m. Note smooth bore with absence of jointing and hole erosion. (c) Depth—39.0 m. Note severe hole caving conditions. (d) Depth—45.7 m. Note open fracture with otherwise smooth hole conditions.

zones can not be made from one drill hole to another. The striations sometimes found on joint and fracture surfaces and the erratic zonation of alteration, fracturing, and brecciation are interpreted as cooling and nonlaminar flow phenomena common to trachytic lave flows in general. Poor core recovery, particularly in the upper portions of the hole probably resulted from jointing, alteration, vesiculation and auto-brecciation, and not from faulting.*

*This view is also expressed by Noble and Hanson (see Ref. 2, p. 7).

Rock Density

Densities of the trachyte porphyry medium are based on laboratory measurements of selected drill cores and rock specimens. Grain densities measured in the laboratory ranged from 2.54 to 2.61 g/cm^3, with an average of 2.58 g/cm^3. These figures represent maximum density values. In situ density of a rock is less than that of individual mineral grains, since it is reduced by porosity, fracturing, and vesiculation. The rock specimen shown in Fig. 6 is a black scoria with an

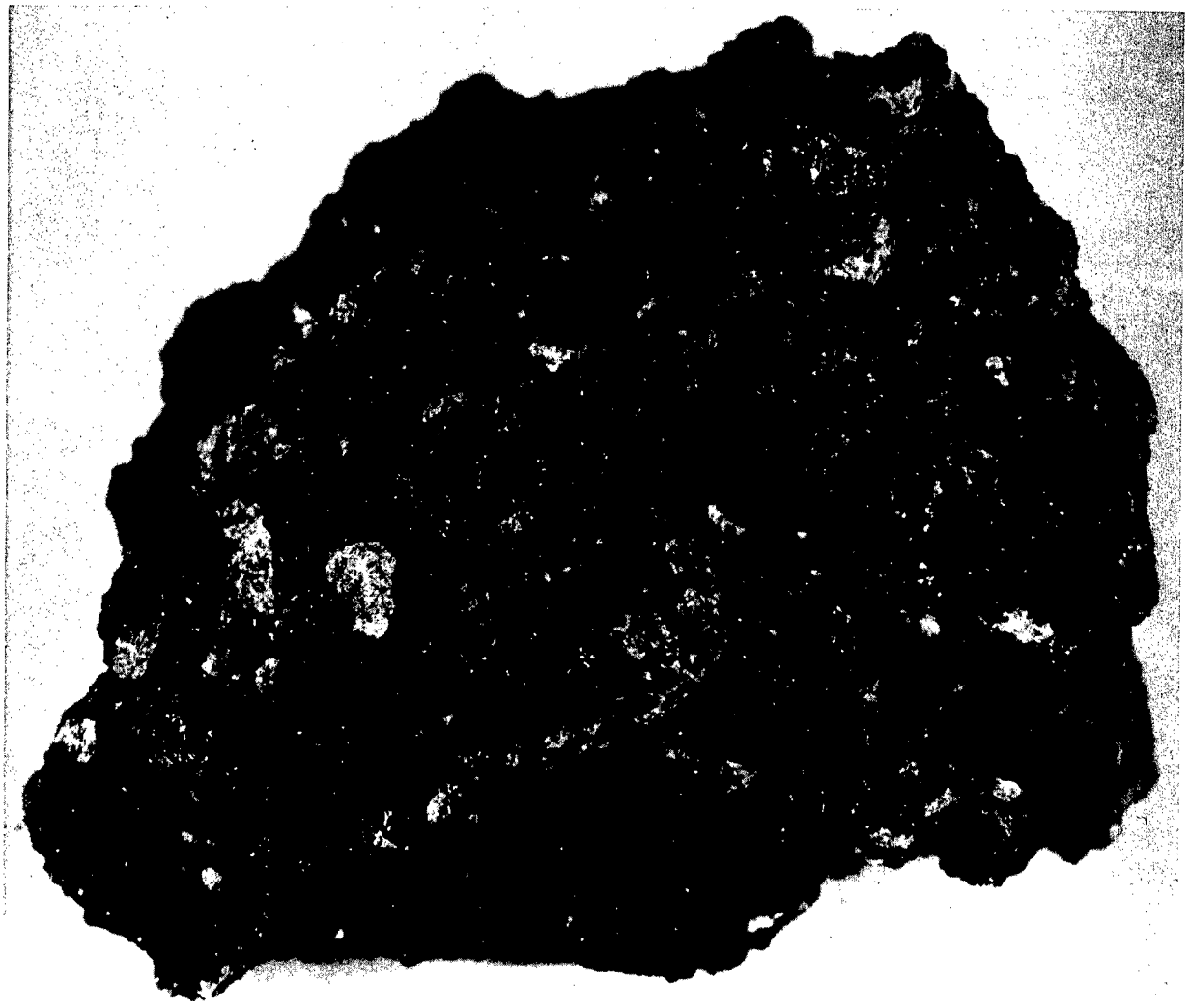

Fig. 6. Rock specimen from vesicular facies of Ribbon Cliff formation.

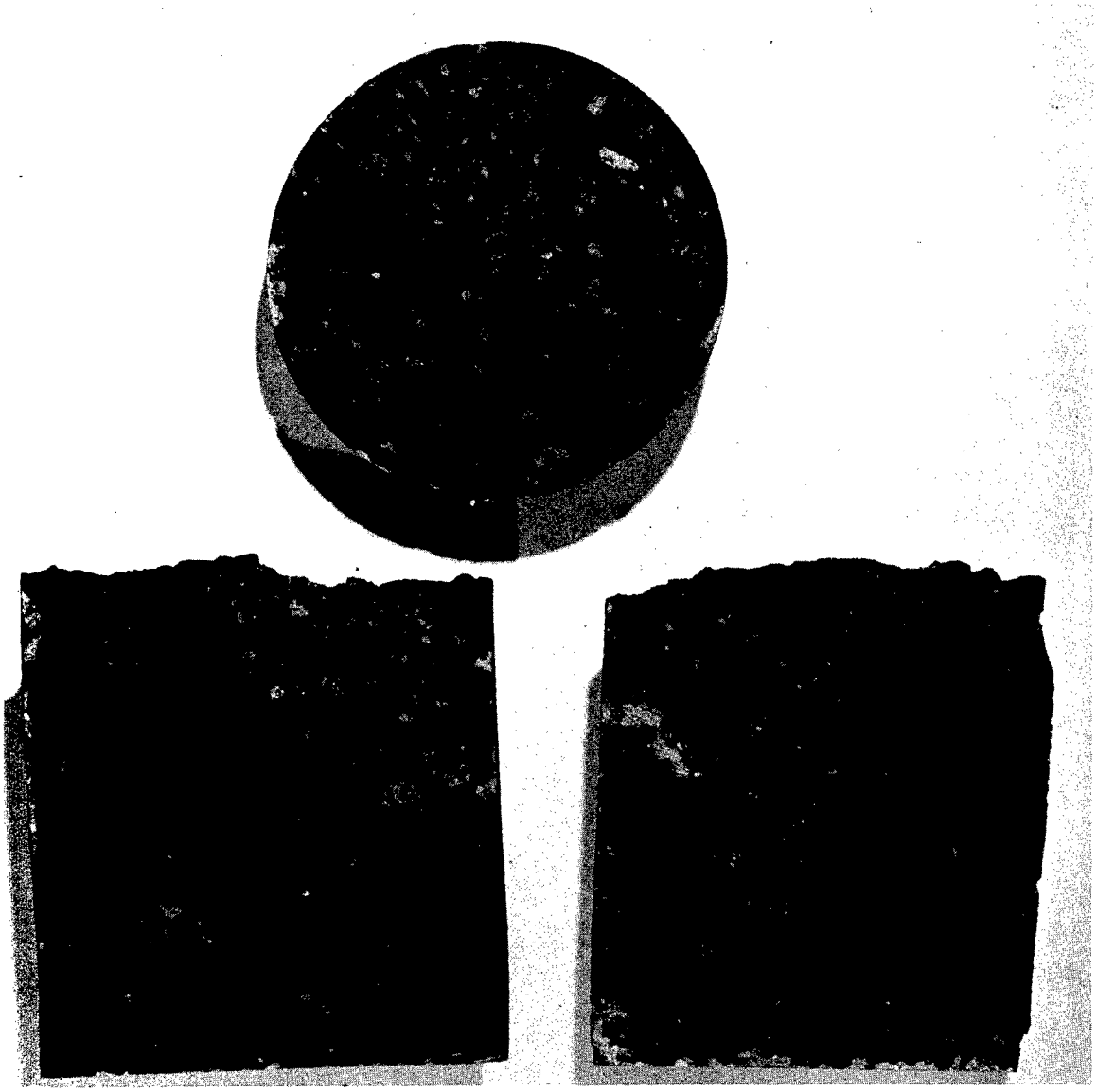

Fig. 7. Typical 3-1/2-in. (8.9-cm) drill cores from dense facies of Ribbon Cliff formation.

estimated porosity of 25%. This specimen was selected as typical of the most highly vesiculated trachyte porphyry at the Palanquin site. The bulk density of this scoria was measured at 1.90 g/cm^3, which probably represents the minimum in situ bulk density, except perhaps for local brecciated zones.

The division of the Ribbon Cliff formation into two facies is based on:

(1) Surface mapping
(2) Laboratory density measurements
(3) Drill cores
(4) Drilling penetration rates
(5) Geophysical logging
(6) Borehole photography

Intermediate gradations exist between the vesiculated and the dense facies. This division represents a working simplification for field and general descriptive use of a structurally complex lithologic environment.

In estimating an average bulk density value* for the dense facies, it is assumed that the bulk densities may approach, but never reach the average grain density value of 2.58 g/cm^3. Natural porosity resulting from fractures, vugs, rock imperfections, and small vesicles tends to reduce bulk density below grain density. Gross in situ porosity was determined to be typically about 5% for the dense facies. Based on this, the average bulk density for the dense facies is estimated to be in the range of 2.4 to 2.5 g/cm^3. Figure 7 shows typical drill cores from the dense facies.

Observations from core, downhole photography, and outcrops indicate that even the most highly vesiculated zones contained lenses and blocks of dense trachyte. From these observations, the in situ bulk porosity for the vesiculated facies is estimated to be typically about 15% plus additional open space from fractures in brecciated zones. The average density for the vesiculated facies is thus estimated to be in the range of 1.9 to 2.2 g/cm^3.

*All in situ values reported are dry bulk density, because of the high permeability of the rock and the depth to the permanent water table.

Logging

General

Conventional geophysical logs used for investigating the Palanquin site were the gamma-gamma density, the caliper, the drilling and coring time, and the percent core recovery logs. These logs were made with instruments furnished and operated by the Welex Divison. In addition, logs were constructed from drilling and coring penetration rates and from percent core recovery. These latter logs are included in this section because they are useful, and even necessary, for interpreting the geology and the physical properties of the media at the Palanquin site.

The variety and accuracy of the geophysical logs used was limited because of the physical condition of the drill holes and the media. Although eight drill holes penetrated the Ribbon Cliff, irregular hole diameter excluded some useful logging probes from four holes. Highly fractured rock prevented the filling of any drill holes with fluid, thereby excluding the use of logging probes which require fluid coupling with the medium.

Density Logs

No useful density information was obtained from the Welex gamma-gamma density logs. The density values of 3.00 to 3.15 g/cm^3 obtained from the gamma-gamma density log are highly improbable. Maximum laboratory grain densities measured by the U. S. Geological Survey, the Waterways Experiment Station,[3] and the LRL-N Geology Group were in the range from 2.54 to 2.61 g/cm^3. This 20% difference between laboratory and log density cannot be explained by higher in situ density caused by additional lithostatic load on the trachyte. Instrument error is the most probable cause of this difference. Figure 8 is a comparison of laboratory density measurements on core, with Welex in situ densities.

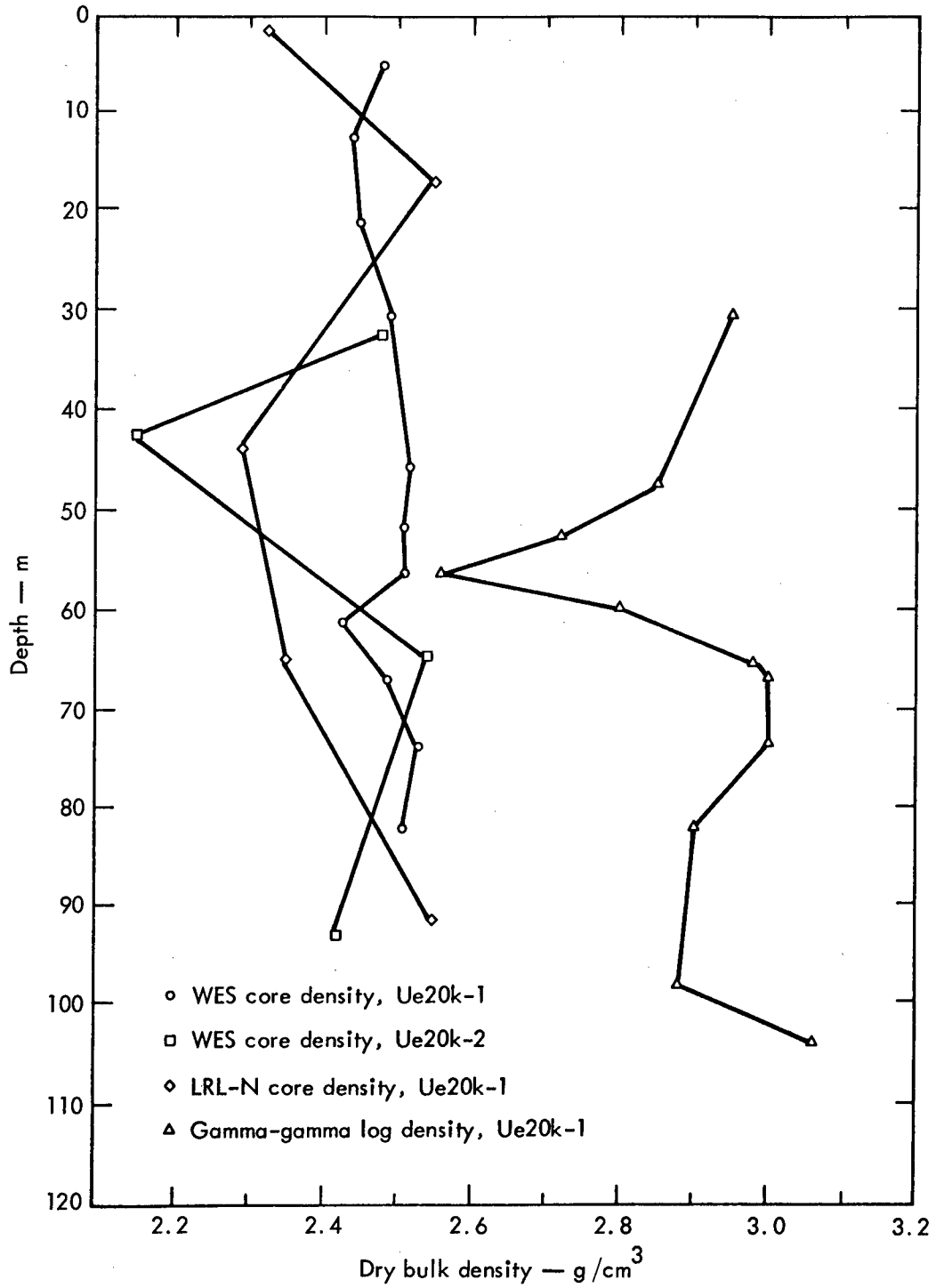

Fig. 8. Comparison of densities from logging and from laboratory measurements on drill core.

Caliper Logging

The hole size was measured with the four-armed, spring-loaded Welex caliper device. The hole size is recorded as a single trace which is the average diameter measured by the four arms. This particular method of hole size measurement has two sources of error which are magnified by bad hole conditions. The recorded caliper log will show a smaller hole size than actual when (1) the tool is not centralized in the hole, or (2) the hole is irregularly shaped.

The four caliper logs of holes U20k, U20k-1, U20k-2, and Ue20k-1 showed extensive zones of extreme hole erosion. Some zones were eroded to greater than three times the drilled size of the hole. Gauge sections of the hole were believed to be indicative of rock competency; eroded zones were indicative of vesiculated, altered, or brecciated trachyte.

Measured hole enlargement ranged upward to at least 140 cm in the 122-cm hole, greater than 69 cm in the 25-cm hole, and 38 cm in the 14-cm hole. No measurements were made in the 7.5-cm holes because the caliper tool was too large to go into these holes. The caliper logs are included in Appendix A.

Drilling and Coring Time Logs

Drilling and coring times are treated as one in this report and are interpreted as being an indication of the relative competency of the trachyte porphyry medium. Slow drilling and coring penetration rates have been used to indicate zones of high fracture frequency, much brecciation, and vesiculation. Comparison of the drilling and coring penetration rates with the caliper logs and cores available indicates that this is a valid interpretation.

Although penetration rates are not normally thought of as physical property measurements, they are a qualitative measure of a rock's relative hardness and competence. The penetration rates are the only measurement which can be cross-compared in all eight holes. The drilling time and coring penetration rate logs are included in Appendix A.

Percent Core Recovery Logs

The percent of core recovery is an indication of rock competency, low core recovery was obtained in fractured, vesiculated, altered, and brecciated zones. Core in zones of incompetent rock tended to break up and wash away during the coring procedure, or to fall out the end of the core barrel while it was being pulled from the hole. No attempt was made to correlate core recovery with physical properties. Core recovery is used here to reinforce data from other downhole methods. Core recovery percentages are included in Appendix A.

Seismic Velocity Measurements

Velocity Measurements

In situ sonic velocity measurements were made in several instrumentation and exploratory holes. Because of the fractured nature of the rock, drilling fluid could not be retained in the holes as a coupling

agent for seismic sources or detectors. Consequently, dry hole logging methods were used.

A seismic uphole method of acquiring high-resolution acoustic wave velocities in dry holes by the means of sand tamping has been used successfully by LRL.[4] For example, it has been found that dry sand in a hole exhibits some characteristics of coupling on a downhole explosive source. Although the coupling efficiency of sand does not approach that of a hydrostatic head and is not especially linear with depth,[5] it nevertheless provides some tamping effect to the explosive, and acts as a buffer between charges hung from a common messenger cable downhole. Seismic uphole velocity measurements were performed by this method.

Velocity Experiments

Two holes were drilled for the purpose of acquiring in situ velocity information. These holes were Ue20k-1 and Ue20k-2. Figure 3 shows the positions of these holes in relation to the emplacement hole, U20k.

The hole designated Ue20k-1 was drilled to a depth of 107 m with a diameter of 14 cm, and located approximately 30 m north of the emplacement hole U20k. Another hole, Ue20k-2 located 280 m southeast of Ue20k-1 was drilled to a nominal depth of 82 m and had a diameter of 7.5 cm. Three experiments were performed in conjunction with these holes to acquire the in situ sonic velocities of the Palanquin medium. A seismic uphole log and refraction measurement were made in Ue20k-1, and a seismic hole-to-hole logging experiment was performed in Ue20k-1 and Ue20k-2.

Seismic Uphole Logging Procedure

Seismic sources consisting of seven 1.36-kg charges of C-4 high explosive attached to a 3.2-mm diam steel messenger cable at 15.2-m intervals were lowered into Ue20k-1. The bottom charge rested at 93.3 m. Some detritus in the bottom of the hole prevented further lowering of the charges, and caused loss of data from the bottom of the holes.

Since the acquisition of velocity data in Ue20k-1 was the first experiment attempted (by the LRL Geophysics Research Group) in a dry hole, grouting the charges in place with cement was thought to be feasible. However, after running down approximately 7.0 m^3 of cement which filled only 39 lineal meters of the hole, it was decided to complete the stemming with sand. The liquid cement was apparently running out into the formation (just above the 67-m level) faster than it could be pumped in. The additional volume of the hole was displaced by dry monterey sand.

The seismic detector of the surface consisted of a Geo-Space HS-10, 2-Hz geophone placed 6 m NW of Ue20k-1. Figure 9 shows in profile the emplacement of sources and detectors.

The recording system electronics consisted of Kintel-114C differential amplifiers, a Honeywell-906 oscillosgraph, and a Tektronix-545 oscilloscope. A 2000-V capacitor discharge unit with a relay-controlled firing function provided the necessary voltage and current to fire the detonators. A voltage divider circuit was used to pulse the Honeywell recorder and trigger the scope for accurate zero times.

Seismic Uphole Logging Results

Of seven shots attempted in Ue20k-1, six functioned properly while the seventh

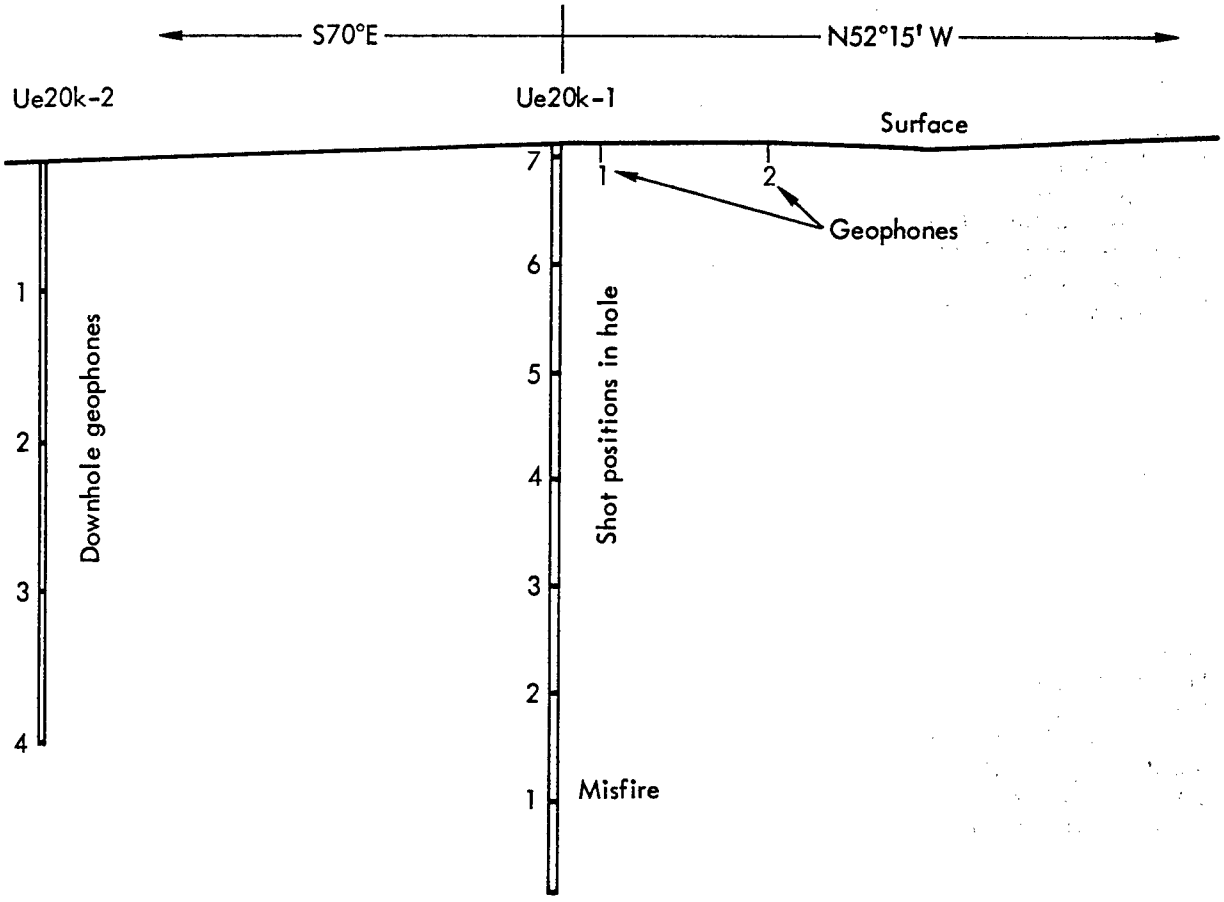

Fig. 9. Detector and shot emplacement profile.

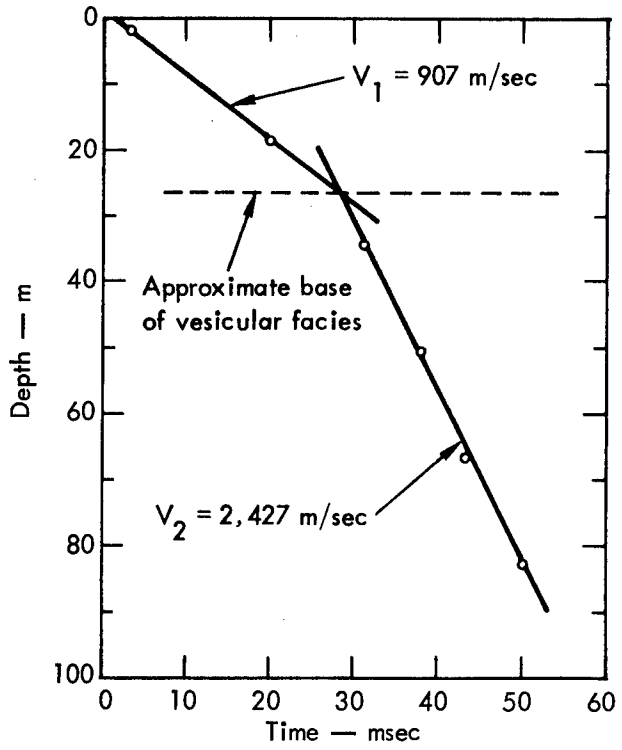

Fig. 10. Average velocity curve from uphole seismic survey.

misfired. Figure 10 is an average velocity curve showing results of the log as seen in Table II. It should be noted that the circles used as points in Fig. 10 have a radius of 500 μsec. These 500-μsec circles represent the limits of probable error in these data.

Table II. Average velocity in Ue20k-1

Depth interval m	Average velocity m/sec
0 - 27	907
27 - 78	2,427

Figure 11 shows the series of oscilloscope records (excluding shot 2 at 78 m) from the uphole velocity survey. Oscillograph records were made as a backup to the scope. From the curve in Fig. 10, it

Shot 3
Depth: 62.7 m
Charge: 3 lb
Geophone offset: 6.09 m
Slant range: 62.7 m
Gain: 0.1 V/cm
Time: 10 msec/cm

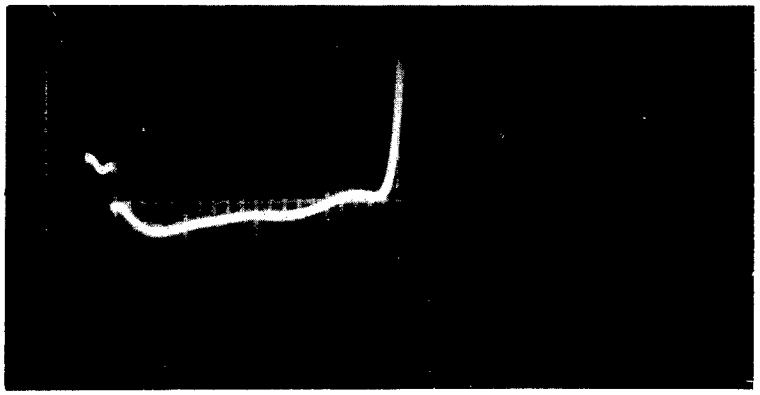

(a)

Shot 4
Depth: 47.5 m
Charge: 3 lb
Geophone offset: 6.09 m
Slant range: 47.9 m
Gain: 0.5 V/cm
Time: 5 msec/cm

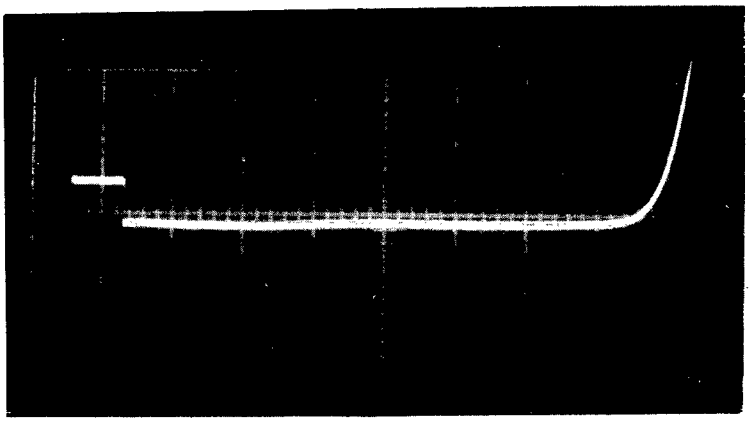

(b)

Shot 5
Depth: 32.3 m
Charge: 3 lb
Geophone offset: 6.09 m
Slant range: 32.9 m
Gain 0.5 V/cm
Time: 5 msec/cm

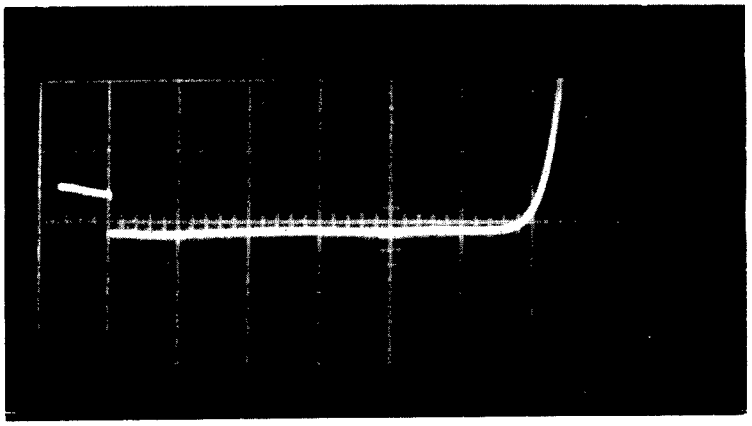

(c)

Fig. 11. Oscillograph records from seismic uphole log in Ue20k-1.

Shot 6
Depth: 17.06 m
Charge: 3 lb
Geophone offset: 6.09 m
Slant range: 18.1 m
Gain: 0.5 V/cm
Time: 5 msec/cm

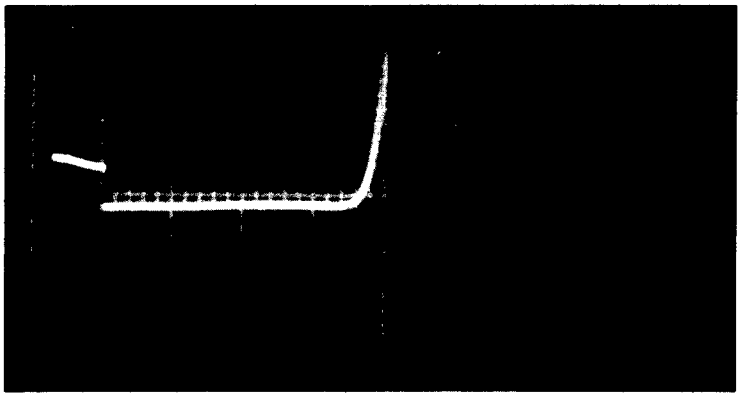

(d)

Shot 7
Depth: 1.8 m
Charge: 3 lb
Geophone offset: 6.09 m
Slant range: 6.37 m
Gain: 0.5 V/cm
Time: 5 msec/cm

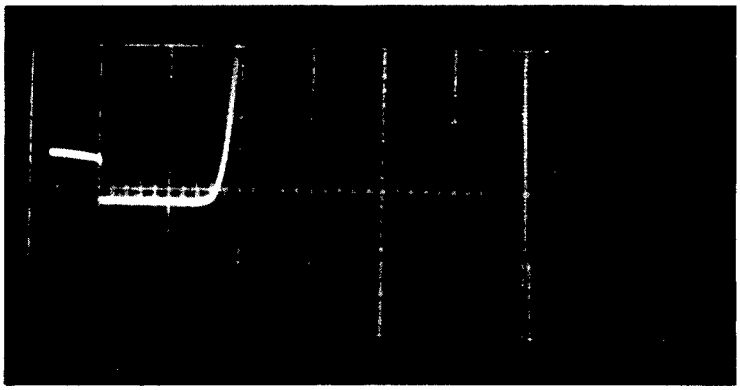

(e)

Fig. 11 (Continued).

is apparent that an acoustic impedance mismatch is present at approximately 27 m. The abrupt average velocity change occurring at this depth should be indicative of a change in lithology and/or the extent of fracturing.

Seismic Hole-To-Hole Logging Procedure

In addition to the uphole survey, Ue20k-2 was instrumented with vertically oriented Geo-Space HS-1, 4.5-Hz geophones in an attempt to measure horizontally traveling P-waves from hole to hole. The geophones were placed in the hole at 21.3 m intervals with the bottom detector resting at 82.3 m. Figure 9 shows the hole-to-hole profile. Dry Monterey sand was poured into the hole to act as an acoustic coupler.

The first arrivals of P-waves (generated from the downhole seismic sources in Ue20k-1 during the uphole logging) were supposed to be detected by the geophones in Ue20k-2.

Seismic Hole-To-Hole Results

Data from this experiment were essentially useless because of arrivals ranging from nonexistent to unintelligible. Possible explanations for the failure may be attributed to:

1. The output signals of the HS-1 transducers were too low (somewhere in

the microvolt range) as a result of the combination of distance and low seismic source yield.

2. Vertically oriented detectors were used in place of horizontal-radially oriented geophones, which were unavailable. When a seismic point source propagates in a spherical mode, and the P-wave has horizontally traveling components, a vertically oriented detector (such as those used in Ue20k-2) does not respond well.

3. Sand stemming probably was insufficient to couple the detectors in their hole.

4. The rock medium is anisotropic. This results in diffraction and refraction of any P-wave in its apparent horizontal travel between holes. Meaningful calculation of arrival times under these circumstances would have been marginal at best.

Seismic Refraction Procedure

A one-shot refraction study was made in order to verify the results of the seismic uphole log with respect to the depth of the velocity discontinuity and velocity in general. This procedure consisted of recording the P-wave travel time for the last shot (in the uphole series) in Ue20k-1 at a depth of 1.8 m to a 2-Hz geophone located on the surface 36.5 m NW of Ue20k-1. The last shot in the uphole series was used for the refraction experiment because it was the shot nearest the surface. When an orthodox refraction profile is made the explosives are ordinarily shot on or very near the surface so that the P-wave can travel down through the medium along a velocity interface, and back up through the medium to a detector.[6]

Seismic Refraction Results

Generally, calculation of a refraction survey yields an average velocity of the medium. However, this particular refraction survey was used to compute (1) the total travel time of the P-wave from shot to detector, and (2) the depth of the velocity discontinuity. These two calculations were performed using the average velocities obtained from the uphole curve in Fig. 10.

Figure 12 is the refraction record made on the Honeywell oscillograph. Trace 1 is the zero time break, Trace 2 is the uphole detector at 6 m from the hole, and Trace 3 is the refraction geophone located 36.5 m from the hole. It should be noted that the first departure (break) from the zero amplitude line of Trace 3 occurs at 0.053 sec. Since the amplitude of this break is small compared with other amplitudes on this trace (no voltages were measured), it appears that vertical motion on the detector is barely perceptible. This suggests that the P-wave travels horizontally almost straight across from the shot to Detector 2, at a velocity of approximately 690 m/sec. This seems reasonable when a velocity of approximately 690 m/sec is assumed from the upper portion of the curve in Fig. 10. Since only two points on this curve are used to average velocity, it is quite possible that an acceleration factor exists between the surface and about 19 m.

The refracted or reflected P-wave energy arrives at Detector 2 at approximately 0.068 sec. As observed from the record in Fig. 12, calculated reflection time from source to detector is about 0.067 sec, and calculated refraction time

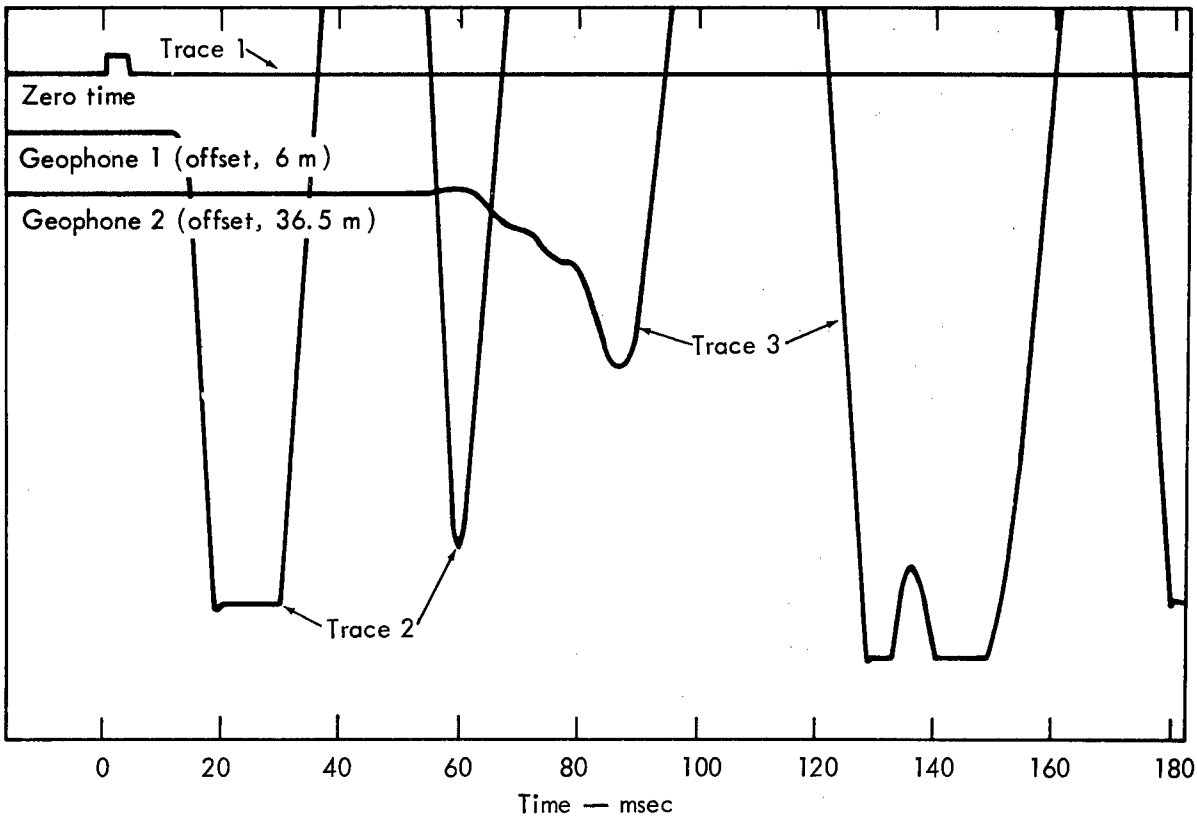

Fig. 12. Oscillograph record for seismic refraction log, uphole survey, Ue20k-1. Shot No. 7: depth, 1.8 m (6.0 ft); charge, 316, time lines, 10 msec; slant range, 6.37 m (20.9 ft).

for the same route is almost 0.065 sec. Since the ΔT between refraction and reflection is so small (about 2 msec and the resolution of this particular event on the record is not high (±2 msec), a positive identification of the event at 0.068 sec would be assumptive.

The last portion of the break (on Trace 3, Fig. 12) at 0.078 sec is the possible arrival of the Rayleigh or surface wave. Since this wave is noted for its large particle displacement and relatively low sonic velocity (about half that of the P-wave) it appears that this event at 0.078 sec meets these specifications. The amplitude of this arrival is higher than that of the others and its average velocity is 468 m/sec, or roughly, one half that of the average P-wave in this area.

Figure 13 is a profile of the refraction and/or reflection path of the P-wave taken in this experiment and is used in the calculation of (1) the total travel time and (2) the depth of velocity discontinuity.

The refraction computation of the total travel time T_t using V_1 = 907 m/sec and V_2 = 2,427 m/sec from the uphole velocity curve should be approximately equal to the observed time of the refraction break on the record in Fig. 10, and is calculated as follows: The critical angle is obtained,

$$\sin \theta_c = \left(\frac{V_1}{V_2}\right).$$

The distance from the shot to the discontinuity and the slant range from the shot to the velocity discontinuity as

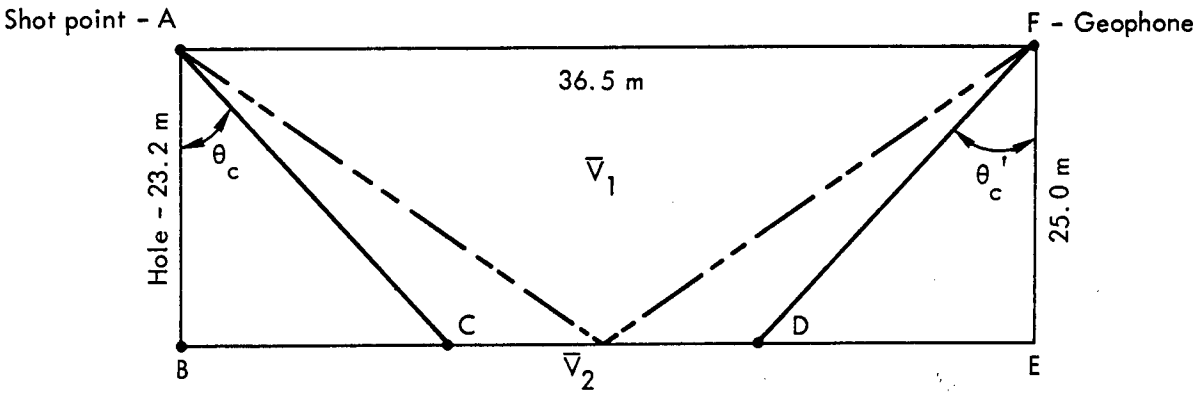

Key

θ_c = Critical angle

AB = Distance from shot to velocity interface (23.2 m)

FE = Distance from geophone to velocity interface (25.0 m)

BE = Surface distance from shot to geophone (36.5 m)

$\overline{V}_1$ = Low-velocity zone, 907 m/sec

$\overline{V}_2$ = High-velocity zone, 2,429 m/sec

T_t = Total travel time

T_l = Travel time in low-velocity medium

T_h = Travel time in high-velocity medium

Fig. 13. Refraction profile of Ue20k-1.

defined by the critical angle can be calculated.

Travel time in the low-velocity medium is:

$$T_1 = \left(\frac{AC}{V_1}\right) + \left(\frac{DF}{V_1}\right),$$

and travel time in the high-velocity medium is:

$$T_h = \left(\frac{CD}{V_2}\right).$$

Therefore, total refracted travel time from source to detector should be

$$T_t = \left(\frac{AC}{V_1}\right) + \left(\frac{CD}{V_2}\right) + \left(\frac{DF}{V_1}\right), \text{ or}$$

T_t + 0.0649 sec.

The reflection theory simply states that the angle of reflection is equal to the angle of incidence. Then, by trigonometry, the distances from the shot to the center of the reflecting layer (velocity discontinuity) and back up to the detector may be computed. Using these distances and V_1 = (907 m/sec), total travel time is 0.0669 sec.

The depth of the velocity discontinuity can be calculated and compared with the above method in Fig. 13 by the following alternate equation form.* This equation may also be compared to Fig. 12.

*Electrodynamic Instrument Corporation, Engineering Data Sheet.

$$D = \frac{\left[T_{ob} - \left(\frac{AF}{V_2}\right) \cos \theta_c\right]}{2\left[\frac{V_2 - V_1 \sin \theta_c}{V_2 V_1}\right]}$$

where,

T_{ob} = Observed refracted travel time (from record) from shot to detector (0.068 sec)

D = Depth of velocity discontinuity

The uphole curve in Fig. 10 shows the discontinuity to be at approximately 27 m, while the above equation corroborates this depth.

In consideration of the calculations and graphic methods of obtaining travel times, depths, and velocities from a simple one-shot refraction or reflection profile as described above, it should be apparent that an acoustic unconformity is definitely present at a depth of approximately 27 m in the vicinity of Ue20k-1

Summary and Conclusions

Geology

The Ribbon Cliff formation at the site consists of trachyte porphyry and is divided into two lithologic facies on the basis of degree of vesiculation and density. These are termed the vesicular facies and the dense facies. The dry bulk density of the vesicular facies is in the range of 1.9 to 2.2 g/cm^3, and the dense facies is in the range of 2.4 to 2.5 g/cm^3. The vesicular facies overlies the dense facies and extends typically 60 m below the ground surface. The facies are locally gradational.

The rock medium is locally jointed, fractured, and brecciated with caliche and clay alteration products deposited in the open spaces. Fragments and blocks of rock, often vesicular and porous, are locally packed together in a latticework of clay. Severe out-of-gauge conditions and poor core recovery in the drill holes were a result of encountering these zones. Evidence of tectonic faulting in the vicinity of SGZ is absent.

Density Logging

The gamma-gamma density tool provided by the on-site logging contractor at the time of the Palanquin Event were oilfield proven tools, and, as such, were more qualitatively than quantitatively oriented. In this case, the 20% discrepancy between the in situ (3.1 g/cm^3) and the core (2.5 g/cm^3) measurements was too high to resolve by natural phenomena; i.e., overburden pressures, stress release, etc.

Much work has gone into the development of high-resolution, proximity-corrected in situ density measuring machines.[7] These new tools now will measure in situ density to within ±2.5%

Seismic Logging

Only one hole (Ue20k-1) was used for the seismic uphole log. But the average velocities of 907 and 2,427 m/sec, plus a velocity discontinuity at approximately 27 m appear genuine. Additional evidence

for the depth of the velocity discontinuity was shown in the refraction experiment.

In situ geophysical measurements in association with nuclear cratering events up to the time of the Palanquin Event were sparse. These measurements and their desired limits of accuracy were largely empirical, and the logging tools and methods capable of high-resolution measurements were unavailable at that time.

References

1. P. P. Orkild and K. A. Sargent, Geologic Map of Pahute Mesa, Nevada Test Site, Nye County, Nevada, U. S. Geological Survey Technical Letter, Special Studies, I-54, August 28, 1967.
2. D. C. Noble and B. V. Hanson, Geology of U20k Site, Area 20, Pahute Mesa, U. S. Geological Survey Technical Letter, Special Studies I-33, March 29, 1965.
3. R. C. Nugent and F. E. Girucky, Preshot Investigations for Project Palanquin, Pahute Mesa, Nevada Test Site, U. S. Army Engineer Waterways Experiment Station, Vicksburg, Mississippi, Report PNE-905F (in press).
4. R. C. Carlson, R. T. Stearns, H. B. Berens, and J. R. Hearst, "High Resolution Uphole Surveys at Lawrence Radiation Laboratory," Geophysics 33, 78 (1968).
5. J. L. Ford, Lawrence Radiation Laboratory, Nevada, private communication (1967).
6. C. H. Dix, Seismic Prospecting for Oil (Harper & Bros., New York, 1952).
7. R. T. Stearns and J. R. Hearst, Geophysical Measurements in a Low Density Medium, Lawrence Radiation Laboratory, Livermore, Rept. UCID-15233 (in publication).

Bibliography

Blankennagel, R. K., U. S. Geological Survey (Water Resources), private communication (1965).

Hackler, W. and Drake, C., "Drilling Records for U20k Exploratory Holes Ue20k-1, Ue20k-2, Ue20k-3, Ue20k-4, and Ue20k-5," U. S. Army Engineer Waterways Experiment Station, Vicksburg, Mississippi, unpublished records, 1965.

Hansen, Spenst M., A Nuclear Crater Formed by a Gas Erosional Mechanism, Lawrence Radiation Laboratory, Livermore, Rept. UCRL-50371, January 1968.

Hill, John H., Crawford, Patrick A, and DeLalla, Oliver F., Chemical Analyses of Post-shot Samples from the Palanquin Event, Lawrence Radiation Laboratory, Livermore, Rept. UCID-15158, June 6, 1967.

Meyer, G. L., and Skrove, J. W., Lawrence Radiation Laboratory, Nevada, private communication, April 1965.

Noble, Donald C., Geologic Map of the Trail Ridge Quadrangle, Nye County, Nevada, U. S. Geological Survey, 1965.

Orkild, P. P., U. S. Geological Survey (Special Projects), private communication (1965).

Orkild, P. P., Monthly Report of Exploration Progress, Pahute Mesa, February 1, 1965, U. S. Geological Survey Technical Letter, Special Studies, January 23, 1967.

Stearns, R. T., Lawrence Radiation Laboratory, Nevada, private communication, March 24, 1965.

Appendix A

Reproduction of Caliper Logs, Drilling Time

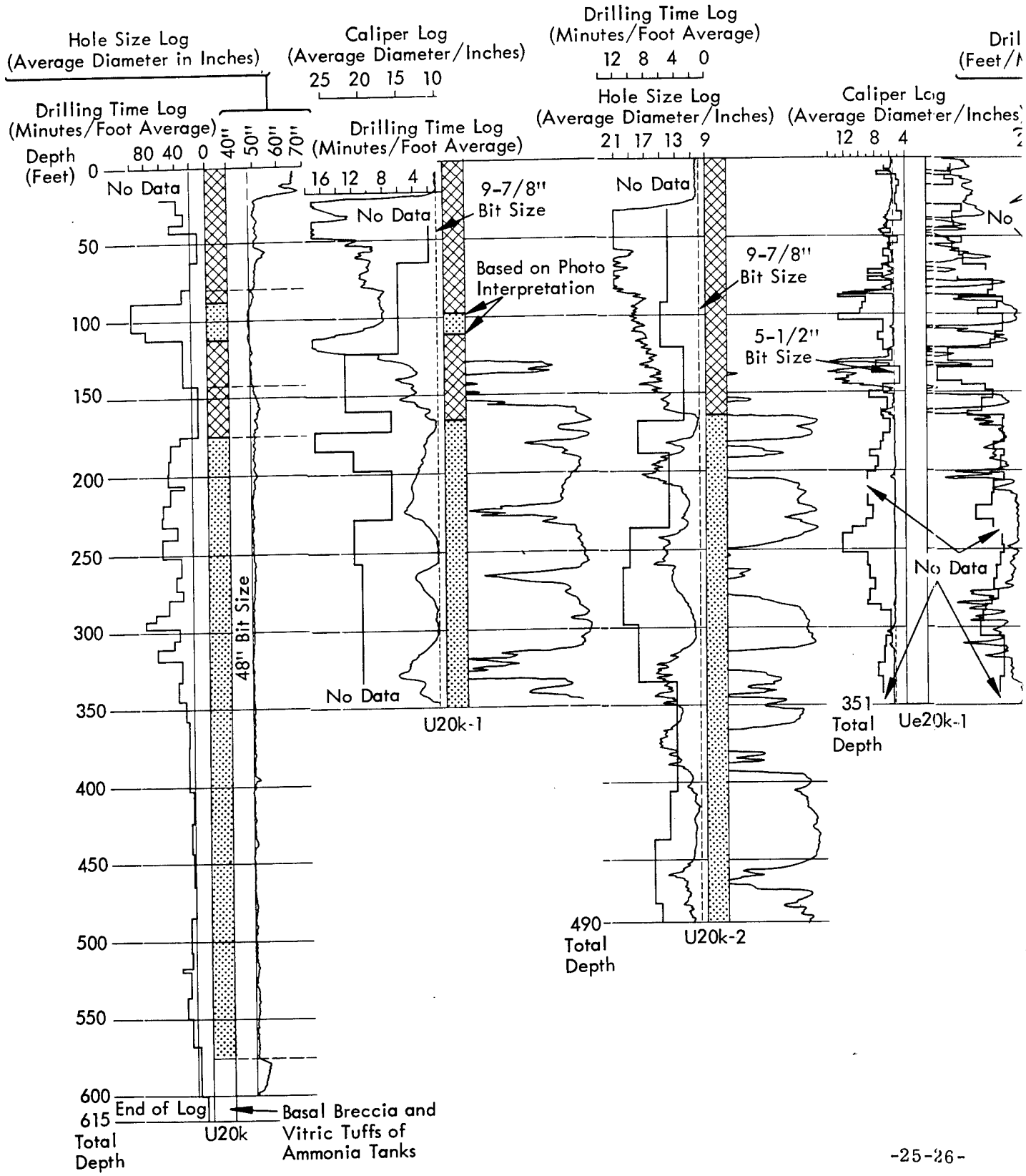

Appendix A

r Logs, Drilling Time Logs, and Core Recovery Logs

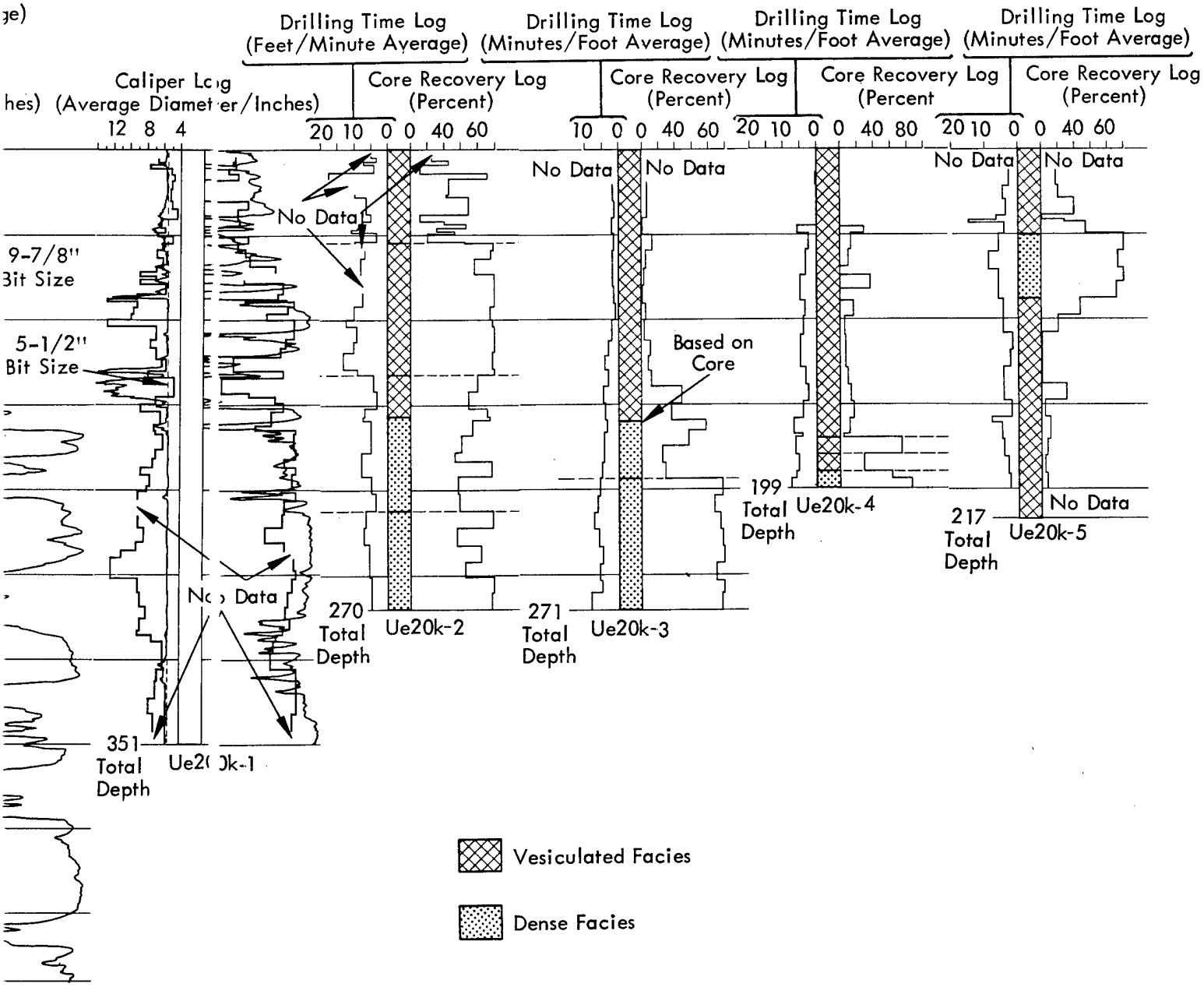

PALANQUIN TECHNICAL REPORTS

Report No.	Agency	Author	Title
PNE-900F	LRL/EGG	R. Rohrer	Ground Motion and Cloud Photography
PNE-901F	LRL	C. Sisemore	Sub-Surface Effects
PNE-902F	SC	L. Vortman	Close-in Air Blast from a Cratering Nuclear Detonation in Rhyolite
PNE-903F	SC	J. Reed	Long-Range Air Blast
PNE-904F	NCG	F. Videon	Crater Topography
PNE-905F	NCG	P. Fisher	Pre-Shot Geological and Engineering Properties Investigations
PNE-906F	LRL/N	L. Meyer	Geophysical Studies
PNE-907F	LRL	T. Gibson et al	Hazards Evaluation Measurements
PNE-908F	EG&G, Inc.	R. Rohrer	Scientific Photography
PNE-909F	LRL	J. Miskel N. Bonner et al	Radiochemical Studies
PNE-910F	USPHS	J. Coogan	Off-Site Surveillance
PNE-911F	REECo	B. Ubanks	On-Site Radiological Safety
PNE-912F	USWB		Weather and Radiation Support Activities
PNE-913F	R. F. Beers Inc.	L. Davis	Analysis of Surface Seismic Data

DISTRIBUTION LIST
(TID-4500, Category UC-35)

No. Copies	
1	AEC ALBUQUERQUE OPERATIONS OFFICE
1	AEC BETHESDA TECHNICAL LIBRARY
25	AEC DIVISION OF PEACEFUL NUCLEAR EXPLOSIVES
1	AEC LIBRARY, WASHINGTON
1	AEC MISSION TO THE IAEA
5	AEC NEVADA OPERATIONS OFFICE
1	AEC NEW YORK OPERATIONS OFFICE
1	AEC PATENT OFFICE
5	AEC SAN FRANCISCO OPERATIONS OFFICE
1	AEC SAVANNAH RIVER OPERATIONS OFFICE
1	AEC SCIENTIFIC REPRESENTATIVE, BELGIUM
1	AEC SCIENTIFIC REPRESENTATIVE, ENGLAND
1	AEC SCIENTIFIC REPRESENTATIVE, JAPAN
1	AEROSPACE CORPORATION, SAN BERNARDINO (AF)
1	AIR FORCE AERO PROPULSION LABORATORY (APE)
1	AIR FORCE FOREIGN TECHNOLOGY DIVISION
1	AIR FORCE INSTITUTE OF TECHNOLOGY
1	AIR FORCE SCHOOL OF AEROSPACE MEDICINE
1	AIR FORCE WEAPONS LABORATORY
1	AMES LABORATORY (AEC)
1	ARGONNE NATIONAL LABORATORY (AEC)
8	ARMY ABERDEEN PROVING GROUND
1	ARMY CHIEF OF ENGINEERS
1	ARMY ELECTRONICS COMMAND
1	ARMY ENGINEER DIVISION
5	ARMY ENGINEER NUCLEAR CRATERING GROUP
6	ARMY ENGINEER WATERWAYS EXPERIMENT STATION
1	ARMY MATERIEL COMMAND
1	ARMY MEDICAL FIELD SERVICE SCHOOL
1	ARMY MEDICAL RESEARCH UNIT
1	ARMY MOBILITY EQUIPMENT RESEARCH AND DEVELOPMENT CENTER
1	ARMY NUCLEAR DEFENSE LABORATORY
1	ARMY PICATINNY ARSENAL
1	ARMY ROCKY MOUNTAIN ARSENAL
1	ARMY SURGEON GENERAL
1	ARMY WALTER REED MEDICAL CENTER
1	ATOMIC POWER DEVELOPMENT ASSOCIATES, INC. (AEC)
2	ATOMICS INTERNATIONAL (AEC)
1	BABCOCK AND WILCOX COMPANY, WASHINGTON (AEC)
2	BATTELLE MEMORIAL INSTITUTE (AEC)
1	BATTELLE-NORTHWEST (AEC)
1	BROOKHAVEN NATIONAL LABORATORY (AEC)
2	BUREAU OF MINES, BARTLESVILLE (INT)
1	BUREAU OF MINES, DENVER (INT)
1	BUREAU OF MINES, LARAMIE (INT)
6	BUREAU OF RECLAMATION (INT)
1	DEPARTMENT OF AGRICULTURE NATIONAL LIBRARY
1	DOD DASA LIVERMORE
1	DOD DASA RADIOBIOLOGY RESEARCH INSTITUTE
1	DOD DASA SANDIA
1	DOD DASA WASHINGTON
1	DU PONT COMPANY, AIKEN (AEC)
1	DU PONT COMPANY, WILMINGTON (AEC)
1	EG&G, INC., ALBUQUERQUE (AEC)
1	EG&G, INC., LAS VEGAS (AEC)
5	EL PASO NATURAL GAS COMPANY
8	ENVIRONMENTAL RESEARCH CORPORATION (AEC)
1	ENVIRONMENTAL RESEARCH CORPORATION, LAS VEGAS (AEC)
1	ENVIRONMENTAL SCIENCE SERVICES ADMINISTRATION, LAS VEGAS (COMM.)
1	ENVIRONMENTAL SCIENCE SERVICE ADMINISTRATION, MARYLAND (COMM.)
1	FRANKFORD ARSENAL (P-D LABS.)
1	GENERAL DYNAMICS/FORT WORTH (AF)
1	GENERAL ELECTRIC COMPANY, CINCINNATI (AEC)
1	GENERAL ELECTRIC COMPANY, SAN JOSE (AEC)
1	GEOLOGICAL SURVEY, DENVER
1	GEOLOGICAL SURVEY, FLAGSTAFF (INT)
1	GEOLOGICAL SURVEY, MENLO PARK (INT)
1	GEOLOGICAL SURVEY (PECORA) (INT)
1	GULF GENERAL ATOMIC INCORPORATED (AEC)
2	HOLMES AND NARVER, INC. (AEC)
1	HUGHES AIRCRAFT COMPANY, FULLERTON (ARMY)
1	INSTITUTE FOR DEFENSE ANALYSIS (ARMY)
1	ISOTOPES, INC. (AEC)
1	JET PROPULSION LABORATORY (NASA)
1	LAWRENCE RADIATION LABORATORY, BERKELEY (AEC)
4	LAWRENCE RADIATION LABORATORY, LIVERMORE (AEC)
2	LOS ALAMOS SCIENTIFIC LABORATORY (AEC)
5	LOVELACE FOUNDATION (AEC)
1	MATHEMATICA (AEC)
1	MUESER, RUTLEDGE, WENTWORTH AND JOHNSTON (AEC)
1	MUTUAL ATOMIC ENERGY LIABILITY UNDERWRITERS (AEC)
1	NASA JOHN F. KENNEDY SPACE CENTER
1	NATIONAL BUREAU OF STANDARDS (LIBRARY)
1	NATIONAL INSTITUTES OF HEALTH (HEW)
1	NATIONAL REACTOR TESTING STATION (INC) (AEC)
1	NAVY ATOMIC ENERGY DIVISION
1	NAVY OFFICE OF NAVAL RESEARCH (CODE 422)
2	NAVY ORDNANCE LABORATORY
1	NAVY ORDNANCE SYSTEMS COMMAND
1	NAVY POSTGRADUATE SCHOOL
1	NAVY RADIOLOGICAL DEFENSE LABORATORY
1	NAVY SHIP SYSTEMS COMMAND HEADQUARTERS
1	NRA, INC.
4	OAK RIDGE NATIONAL LABORATORY (AEC)
1	OCEANOGRAPHIC SERVICES, INC. (AEC)
1	OHIO STATE UNIVERSITY (OCD)
3	PUBLIC HEALTH SERVICE, LAS VEGAS (HEW)
1	PUBLIC HEALTH SERVICE, MONTGOMERY (HEW)
1	PUBLIC HEALTH SERVICE, ROCKVILLE (HEW)
1	PUBLIC HEALTH SERVICE, WINCHESTER (HEW)
1	PUERTO RICO NUCLEAR CENTER (AEC)
1	PURDUE UNIVERSITY (AEC)
1	RADIOPTICS, INC. (AEC)
2	REYNOLDS ELECTRICAL AND ENGINEERING COMPANY, INC. (AEC)
4	SANDIA CORPORATION, ALBUQUERQUE (AEC)
1	SANDIA CORPORATION, LIVERMORE (AEC)
1	SOUTHWEST RESEARCH INSTITUTE (AEC)
1	STANFORD UNIVERSITY (AEC)
1	TENNESSEE VALLEY AUTHORITY
1	UNION CARBIDE CORPORATION (ORGDP) (AEC)
1	UNIVERSITY OF CALIFORNIA, DAVIS, TALLEY (AEC)
1	UNIVERSITY OF MICHIGAN (VESIAC) (ARMY)
1	UNIVERSITY OF ROCHESTER (KAPLON) (AEC)
1	UNIVERSITY OF TENNESSEE (AEC)
1	UNIVERSITY OF WASHINGTON (AEC)
1	WASHINGTON STATE UNIVERSITY (AEC)
1	WESTINGHOUSE ELECTRIC CORPORATION, MC KENNA (AEC)
66	AEC DIVISION OF TECHNICAL INFORMATION EXTENSION
25	CLEARINGHOUSE FOR FEDERAL SCIENTIFIC AND TECHNICAL INFORMATION